



An alginate-based hybrid system for growth factor delivery in the functional repair of large bone defects

Yash M. Kolambkar^{a,1}, Kenneth M. Dupont^{b,2}, Joel D. Boerckel^{b,2}, Nathaniel Huebsch^{c,3}, David J. Mooney^{d,4}, Dietmar W. Hutmacher^{e,5}, Robert E. Guldberg^{b,*}

^aWallace H. Coulter Department of Biomedical Engineering, Parker H. Petit Institute for Bioengineering and Bioscience, Georgia Institute of Technology, 315 Ferst Dr, Atlanta, GA 30332, USA

^bGeorge W. Woodruff School of Mechanical Engineering, Parker H. Petit Institute for Bioengineering and Bioscience, Georgia Institute of Technology, 315 Ferst Dr, Atlanta, GA 30332, USA

^cSchool of Engineering and Applied Sciences, Harvard-MIT Division of Health Sciences and Technology, Harvard University, 29 Oxford St., 319 Pierce Hall, USA

^dSchool of Engineering and Applied Sciences, Wyss Institute for Biologically Inspired Engineering, Harvard University, 29 Oxford St., 319 Pierce Hall, USA

^eInstitute of Health and Biomedical Innovation, Queensland University of Technology, George W. Woodruff School of Mechanical Engineering, Georgia Institute of Technology, 60 Musk Avenue, Kelvin Grove QLD 4059, Australia

ARTICLE INFO

Article history:

Received 18 August 2010

Accepted 27 August 2010

Available online 22 September 2010

Keywords:

Bone regeneration

Drug delivery

Bone morphogenetic protein

Scaffold

Nanofiber mesh

Alginate

ABSTRACT

The treatment of challenging fractures and large osseous defects presents a formidable problem for orthopaedic surgeons. Tissue engineering/regenerative medicine approaches seek to solve this problem by delivering osteogenic signals within scaffolding biomaterials. In this study, we introduce a hybrid growth factor delivery system that consists of an electrospun nanofiber mesh tube for guiding bone regeneration combined with peptide-modified alginate hydrogel injected inside the tube for sustained growth factor release. We tested the ability of this system to deliver recombinant bone morphogenetic protein-2 (rhBMP-2) for the repair of critically-sized segmental bone defects in a rat model. Longitudinal μ -CT analysis and torsional testing provided quantitative assessment of bone regeneration. Our results indicate that the hybrid delivery system resulted in consistent bony bridging of the challenging bone defects. However, in the absence of rhBMP-2, the use of nanofiber mesh tube and alginate did not result in substantial bone formation. Perforations in the nanofiber mesh accelerated the rhBMP-2 mediated bone repair, and resulted in functional restoration of the regenerated bone. μ -CT based angiography indicated that perforations did not significantly affect the revascularization of defects, suggesting that some other interaction with the tissue surrounding the defect such as improved infiltration of osteo-progenitor cells contributed to the observed differences in repair. Overall, our results indicate that the hybrid alginate/nanofiber mesh system is a promising growth factor delivery strategy for the repair of challenging bone injuries.

© 2010 Elsevier Ltd. All rights reserved.

1. Introduction

Autologous and allogeneic bone grafting are the most widely used treatment modalities for fracture non-unions and large bone

defects [1,2]. However, these techniques are associated with a number of drawbacks, including the limited graft material available for autografts and the high failure rate of allografts [3–5]. These limitations have stimulated the search for improved techniques for bone repair, and tissue engineering/regenerative medicine (TE/RM) strategies have demonstrated significant potential in developing bone graft substitutes [6,7]. These approaches promote tissue repair by providing a combination of physical and biochemical cues through structural scaffolds and biologics [8–10].

Much of bone TE/RM research is focused on the use of three-dimensional scaffolds having adequate strength to support *in vivo* loading [11–13]. However, these structural scaffolds are difficult to design and fabricate at high porosity. They usually do not provide an optimal environment for cellular function and many suffer from slow resorption kinetics, thereby impeding

* Corresponding author. Tel.: +1 404 894 6589; fax: +1 404 385 1397.

E-mail addresses: yash.kolambkar@gmail.com (Y.M. Kolambkar), kennethmdupont@yahoo.com (K.M. Dupont), joel.boerckel@gmail.com (J.D. Boerckel), nhuebsch@fas.harvard.edu (N. Huebsch), mooneyd@seas.harvard.edu (D.W. Mooney), dietmar.hutmacher@qut.edu.au (D.W. Hutmacher), robert.guldberg@me.gatech.edu (R.E. Guldberg).

¹ Tel.: +1 404 933 8512; fax: +1 404 385 1397.

² Tel.: +1 404 385 1327; fax: +1 404 385 1397.

³ Tel.: +1 617 495 1689.

⁴ Tel.: +1 617 384 9624.

⁵ Tel.: +61 7 3138 6077; fax: +61 7 3138 6030.

functional restoration of the damaged tissue. We previously demonstrated, for example, that poly(L/DL-lactide) scaffolds infused with recombinant human bone morphogenetic protein-2 (rhBMP-2) promoted bone ingrowth but failed to fully restore the mechanical properties of long bone defects [11]. Thin, two-dimensional membranes have been used to promote bone repair by placing them along the periosteal surface to demarcate the osseous from the non-osseous region [14–17]. This technique, termed guided bone regeneration, has been applied successfully in the oral and maxillofacial fields to regenerate lost alveolar and skull bone [18–20]. However, few studies have investigated the use of polymer membranes in the treatment of large defects in load-bearing bones, and none have quantitatively evaluated the restoration of limb function [21–23].

Electrospun nanofiber meshes have recently emerged as a new generation of scaffold membranes, possessing a number of features suitable for tissue regeneration [24,25]. They have fibers of the same size-scale of extracellular matrix (ECM) components (fiber diameters ranging from nanometer to sub-micrometer) and a large surface area, which may improve cellular attachment, morphology, migration and function. Nanofiber meshes have been shown to support osteogenic differentiation of progenitor and stem cells *in vitro* [26–29], and have been tested in calvarial defect models *in vivo* [30,31]. However, their efficacy in guiding long bone regeneration *in vivo* remains to be investigated.

Though a scaffold provides a template for guiding bone regeneration, biologic factors such as cells, growth factors or genes are typically required to effectively regenerate challenging bone defects [11,32]. Osteoinductive growth factors like rhBMP-2 have demonstrated some clinical success for bone healing, but large doses are needed [33,34]. Delivery systems that provide sustained release and improved local retention may provide efficacy at lower protein dose, thereby minimizing complications and making the therapy more cost effective [35–38]. Alginate hydrogels, made from brown algae derived polysaccharides, have been established as a scaffolding material [39] and a spatio-temporal delivery vehicle for a wide range of proteins [40–42]. Though mammalian cells lack receptors for alginate polymers, the alginates can be covalently coupled with adhesion peptides to promote cellular attachment [43]. In addition, the degradation rate of these hydrogels can be increased by Gamma-irradiation, resulting in lower molecular weight polymers. These modified alginates have been demonstrated to be better suited for TE/RM applications by allowing faster ingrowth of cells and tissue [39,44].

The primary objective of this study was to develop and test a hybrid growth factor delivery system for bone repair that utilizes an injectable alginate hydrogel for protein delivery and an electrospun nanofiber mesh for guiding bone regeneration. To test this system, we evaluated its ability to deliver rhBMP-2 for the repair of critically-sized segmental bone defects *in vivo*. For control group comparisons, we also examined the ability of the nanofiber mesh alone, and in combination with alginate hydrogel, to heal the bone defects without rhBMP-2. Furthermore, the effect of a perforated nanofiber mesh design on bone repair was investigated. We hypothesized that rhBMP-2 delivery in the nanofiber mesh/alginate system would promote bone ingrowth and fully restore the mechanical properties of 8 mm segmental bone defects in the rat model. We further hypothesized that the perforated nanofiber mesh design would accelerate bone ingrowth due to enhanced early defect vascularization. We tested our hypothesis in an *in vivo* test bed model that utilizes quantitative techniques to assess differences in bone and vascular regrowth and restoration of mechanical function.

2. Materials and methods

2.1. Fabrication of nanofiber mesh tubes

Poly(ϵ -caprolactone) (PCL) pellets (Sigma–Aldrich, St. Louis, MO) were dissolved in a 90:10 volume ratio of hexafluoro-2-propanol (HFP):dimethylformamide (DMF) (Sigma–Aldrich) to obtain a 12% (w/v) polymer solution. DMF was first slowly added to HFP to prevent excessive heat generation, and mixed well on a stir plate for 5 min. The PCL pellets were then added to the solvent solution, and gently stirred for 16–24 h. The solution was visually inspected to ensure a homogeneous and clear solution. The polymer solution was loaded in a 3 mL syringe (Becton–Dickinson, Franklin Lakes, NJ), and a 22 gauge blunt stainless steel needle (Jensen Global Inc., Santa Barbara, CA) was attached to the syringe end. The syringe was mounted on a syringe pump (Harvard Apparatus, Holliston, MA) set at a rate of 0.75 mL/h. The fibers were collected on a flat copper plate (McMaster–Carr, Atlanta, GA), which was placed at a distance of 20–23 cm from the needle end. Fibers were electrospun for 5 h at a voltage of 13–20 kV, supplied by a high voltage power supply (Gamma High Voltage Research, Ormond Beach, FL), to obtain a thick sheet of nanofiber mesh. The residual solvent from the meshes was allowed to evaporate by placing them in a desiccator overnight. The morphology of the nanofiber meshes was examined using a Scanning Electron Microscope (SEM; Hitachi HTA, Pleasanton, CA) after gold coating using a sputter coater (Quorum Technologies, East Granby, CT). The diameter of the fibers were quantified by analyzing the SEM images (at 7000 \times magnification) using a custom MATLAB[®] (The MathWorks Inc., Natick, MA) code.

The nanofiber meshes, as fabricated above, were used to create tubular implants. Rectangular samples measuring 13 \times 19 mm were cut from a mesh. In some samples, perforations spaced approximately 1.5 mm apart were made in the mesh using a 1 mm diameter biopsy punch (Miltex Inc., York, PA). The rectangular mesh samples were wrapped around a steel mandrel (McMaster–Carr) to form a tube having a diameter of approximately 5 mm and 13 mm length. The overlapping edges of the mesh were secured together by using UV glue (DYMEX Corporation, Torrington, CT), which was cured with a LED spot curing lamp (DYMEX Corporation). The nanofiber mesh tubes were then rinsed twice in 70% alcohol (VWR, West Chester, PA), and sterilized by submerging in 200 proof ethanol (Sigma–Aldrich) and allowing the ethanol to evaporate overnight. After the samples had dried completely, they were pre-wetted with sterile 70% ethanol for 30 min. After aspirating the 70% ethanol, the mesh tubes were rinsed three times with excess phosphate-buffered saline (PBS; Mediatech Inc., Manassas, VA), and placed in α MEM (Invitrogen) until implantation.

2.2. Preparation of alginate hydrogel with and without growth factors

Irradiated RGD-modified alginates were prepared as described previously [44]. Briefly, MVG sodium alginate (FMC Biopolymer, Princeton, NJ) was subjected to a 5 Mrad dose of gamma-irradiation. This reduces the molecular weight of the polymer leading to a faster degradation rate, which makes it more appropriate for *in vivo* studies [39]. The irradiated alginates were then covalently coupled with G₄RGDASSP peptide sequences (Peptides International, Kentucky, LA) at a density of 2 sequences per polymer chain using standard carbodiimide chemistry [45]. The resulting RGD-alginates were sterile filtered, lyophilized and stored at –20 °C.

To prepare hydrogels, the RGD-alginates were reconstituted in α MEM to obtain a 2.5% (w/v) solution. Lyophilized rhBMP-2 (R&D Systems, Minneapolis, MN) was reconstituted in 0.1% rat serum albumin (RSA; Sigma–Aldrich) made in 4 mM HCl, at a concentration of 200- μ g/mL. The alginate solution was then mixed with the rhBMP-2 solution at a ratio 5:1 (700 μ L alginate solution @2.5% (w/v) with 175 μ L rhBMP-2 @200 μ g/mL). This results in a 2% (w/v) alginate solution containing 40 μ g/mL rhBMP-2. The rhBMP-2 containing alginate solution was cross-linked with a calcium sulfate (Sigma–Aldrich) slurry (0.21 g CaSO₄ per 1 mL deionized water) at a ratio of 25:1 (35 μ L of CaSO₄ with 875 μ L of alginate/rhBMP-2 solution). The mixing was performed in two 1 mL syringes (Becton–Dickinson, Franklin Lakes, NJ) coupled with a syringe connector (Cole–Parmer, Vernon Hills, IL) with Luer-Lok fittings to minimize air bubbles. Another set of hydrogels was prepared without rhBMP-2 by substituting the rhBMP-2 solution with the carrier (0.1% RSA) alone. The alginate solutions were allowed to gel in the syringes for 30 min at room temperature and then transferred to 4 °C. The hydrogels were kept at 4 °C overnight and used in surgery the following day. Aseptic conditions were maintained in all the above steps, including handling of the exterior of the syringe.

2.3. rhBMP-2 release kinetics

RGD-alginate solutions containing rhBMP-2 were cross-linked with calcium sulfate slurry as above, and immediately injected into custom designed molds containing 4 mm diameter wells. The alginate solutions were allowed to gel for 30 min at room temperature, producing cylindrical plugs measuring 4 mm in diameter and 8 mm in length. Each cylindrical alginate plug contained 500 ng rhBMP-2. Following a brief rinse in 0.1 M CaCl₂ (Sigma–Aldrich), the samples were incubated at 37 °C in 1-mL PBS containing calcium and magnesium ions. At specific time points through day 21, the entire buffer solution was collected and replaced with fresh 1-mL PBS. On days 0 and 21, alginate specimens were dissolved by immersing in 8-mL and 2-mL, respectively, of 2% (w/v) sodium citrate (Sigma–Aldrich) for 30 min at room

temperature. The amount of rhBMP-2 present in the collected PBS and sodium citrate solution was quantified using an ELISA kit (R&D Systems), following the manufacturer's instruction.

2.4. Surgical procedure and analysis

An established critically-sized, femoral segmental defect rat model was used in this study. All surgical procedures were approved by the Institutional Animal Care and Use Committee (IACUC protocol #A05041) at the Georgia Institute of Technology. The rat model and surgical technique has been described previously [11]. Briefly, bilateral 8 mm segmental defects were created in the mid femoral diaphyses of 13-week old female Sasco Sprague–Dawley rats. Prior to defect creation, the femora were stabilized by modular fixation plates consisting of a polysulfone plate and two stainless steel plates (Fig. 1E). This is a more challenging repair model compared to the 5–6 mm segmental defect models that are typically used in rats. Nanofiber mesh tubes were placed around the adjacent bone ends such that the tube lumen contained the defect and there was an overlap of 2.5 mm with the native bone ends at each end of the tube. In some groups, 125 μ L pre-gelled 2% alginate with or without 5 μ g rhBMP-2 was injected in the tube lumen using a 22 g needle (Jensen Global Inc.). The pre-gelled alginate is ejected from the needle in a continuous thin filament shape and fits compactly inside the tube. The tubes used for one of the groups had 1 mm diameter perforations to enhance vascular invasion during the repair process. The four groups ($n = 6-8$) were as follows (Table 1): (I) Mesh alone, (II) Mesh with alginate, (III) Mesh with alginate containing rhBMP-2, (IV) Perforated mesh with alginate containing rhBMP-2. The groups were assigned to the right and left limbs to evenly distribute pairs of groups and obtain a balanced experimental design. After surgery, the animals were allowed to recover and move freely. For pain relief, the animals were injected with 0.03 mg/kg buprenorphine subcutaneously every 8 h for the first 48 h and 0.01 mg/kg buprenorphine for the next 24 h. Radiographs and *in vivo* micro-computed tomography (μ CT) images were obtained at 4 and 12 weeks after surgery to evaluate bone healing. The rats were euthanized at 12 weeks and femora were extracted for mechanical testing. Histological analysis was performed on femora extracted at 4 and 12 weeks.

2.5. 2-D radiographs and 3-D *in vivo* μ CT imaging

At 4 and 12 weeks after implantation, two-dimensional radiographs (Faxitron MX-20 Digital, Faxitron X-ray Corp., Wheeling, IL) of the femur were taken to qualitatively assess bone regeneration and defect bridging. For the quantitative evaluation of bone formation, *in vivo* μ CT was performed at the same time points. The rats were anesthetized by isoflurane and placed in an *in vivo* μ CT system (Viva-CT, Scanco Medical, Bassersdorf, Switzerland). The femoral defect region was scanned at a 38.5 μ m voxel resolution, a voltage of 55-kVp and a current of 109 μ A. The radio-translucent polysulfone plate does not interfere with μ CT scanning and therefore allows longitudinal evaluation of bone ingrowth. To obtain a consistent volume of interest (VOI) between animals and to avoid including the native bone ends, only the central 4 mm of the 8 mm defect was analyzed *in vivo* by drawing circular contours. A Gaussian filter (sigma = 1.2, support = 1) was used to suppress noise in the VOI, and a global threshold corresponding to a density of 270.3 mg hydroxyapatite/cm³ was applied to obtain the regenerated bone volume. This threshold was selected by the visual inspection of individual scan slices to detect newly formed bone and to exclude soft tissues, the polysulfone fixation plate and the nanofiber mesh tube. The segmented images were then used to determine bone volume and density within the defined VOI within each defect. In addition, a density map was calculated in the segmented bone volume, and presented as a pseudo color-scaled image.

2.6. Torsional testing

The freshly extracted femora at 12 weeks were wrapped in gauze moistened with PBS, and stored at -20° C. Just before testing, samples were thawed in PBS and the majority of soft tissues adjacent to the bone removed. The ends of the femur were embedded in end blocks using Wood's metal (Alfa Aesar, Wood Hill, MA) and aligned using a custom fixture. The polysulfone plate was then detached from the metal plates to enable loading of the bone. The potted femur was loaded into holding brackets mounted on a Bose ElectroForce system (ELF 3200, Bose EnduraTEC, Minnetonka, MN) fitted with a 2 Nm torsional load cell. The samples were rotated to failure at a rate of 3 $^{\circ}$ per second under displacement control, and the torque and rotation were recorded. Maximum torque was calculated by locating the

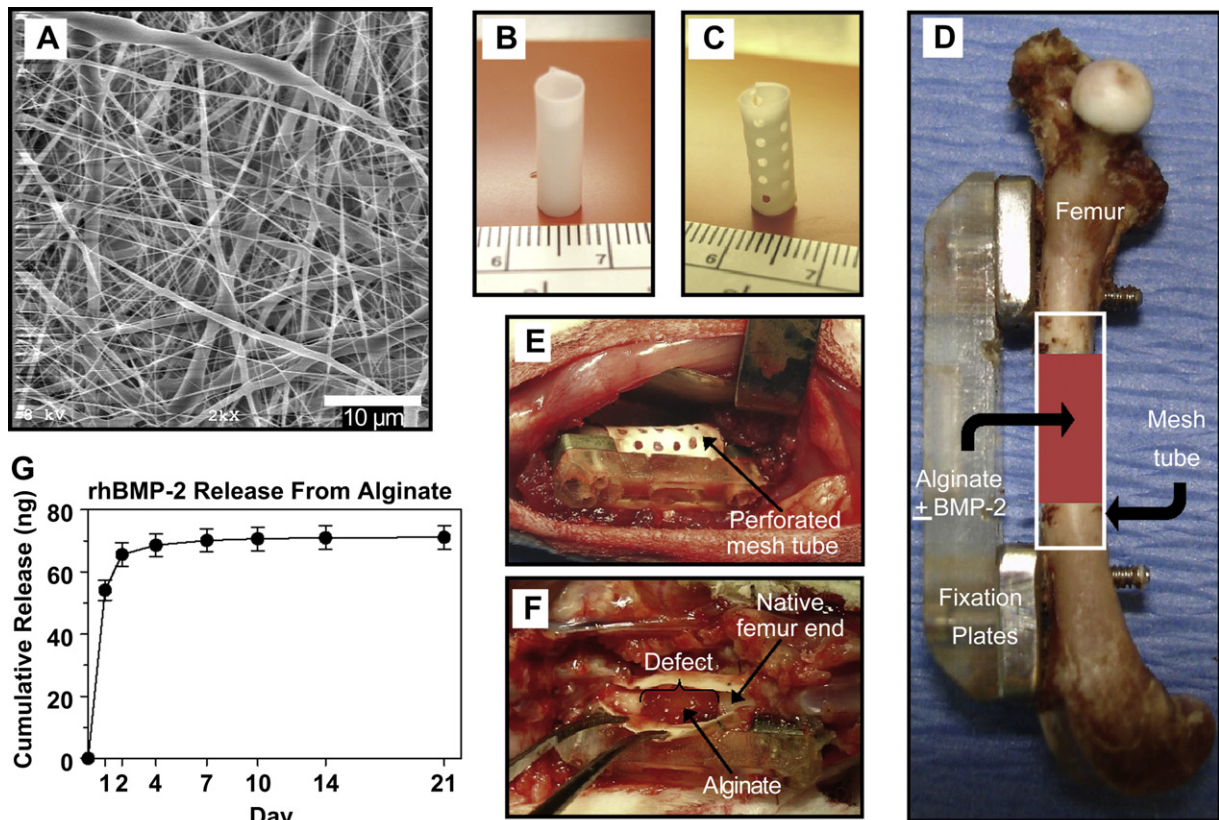


Fig. 1. (A) Nanofiber mesh tubes and alginate hydrogel for surgery. SEM image of electrospun nanofiber mesh illustrating the smooth and bead-free nano-scaled fibers. (B) Hollow tubular implant without perforations made from nanofiber meshes. (C) Tubular implant with perforations. (D) Scheme of implant in segmental bone defect. Modular fixation plates are used to stabilize the femur. A nanofiber mesh tube is placed around the 8 mm defect. In some groups, alginate hydrogel, with or without rhBMP-2 is injected inside the hollow tube. (E) Picture of defect after placement of a perforated mesh tube. The alginate inside the tube can be seen through the perforations. (F) A specimen was taken down after 1 week and the mesh tube was cut open. The alginate was still present inside the defect, with hematoma present at the bone ends. (G) Alginate release kinetics over 21 days *in vitro*. Sustained release of the rhBMP-2 was observed during the first week.

Table 1

The four groups utilized in the *in vivo* study, with the implant conditions in each group.

| Group # | Nanofiber mesh tube | Perforations | Alginate | rhBMP-2 |
|---------|---------------------|--------------|----------|---------|
| I | + | – | – | – |
| II | + | – | + | – |
| III | + | – | + | + |
| IV | + | + | + | + |

failure torque, which occurred within the first 15° for bridged defects. Samples that did not bridge displayed a gradual increase in torque and the absence of a sharp failure point, due to soft tissue stretching. For these samples, the failure torque was measured in the first 60° to avoid analyzing the forces generated due to the stretching of soft tissues. Stiffness was calculated by finding the slope of the straight line fitted to the linear portion of the torque–rotation plot before failure.

2.7. Histological analysis

One representative sample from each group was selected for histological evaluation at 4 and 12 weeks. The extracted femora were fixed in 10% neutral buffered formalin for 48 h. They were dehydrated in a series of alcohol solutions of increasing concentrations, infiltrated with methyl methacrylate (MMA), and embedded by polymerizing the MMA. Ground sections, 50–80 µm thick, were generated using an EXAKT Grinding System (EXAKT Technologies, Oklahoma City, OK). The sections were stained with Sanderson's Rapid Bone Stain [46] and a van Gieson counter stain (SURGIPATH Medical Inc., Richmond, VA, USA). This stain permits the detection of bone (pink), muscle (blue green) and cells (blue).

2.8. Analysis of vascularity during bone regeneration

The vascular regrowth at the defect area was investigated at 3 weeks post-surgery by using a modified version of a previously described µCT-based angiography technique [12,47]. After induction of anesthesia using isoflurane, a 25 gauge catheter was introduced into the abdominal aorta and 250 units (0.25 mL of 1000 units/mL) heparin

were injected. The rat hind limb vasculature was cleared with PBS, fixed with 10% neutral buffered formalin and cleared again with PBS using a peristaltic pump (Masterflex, Cole–Parmer). The rats were euthanized by an overdose of isoflurane before the formalin perfusion. A radiopaque, lead chromate based contrast agent (Flow Tech, Carver, MA) was then injected and allowed to polymerize for at least 2 h. The femur along with its musculature was excised carefully, fixed in 10% neutral buffered formalin for 48 h, and decalcified for 2 weeks using a formic acid based solution (Cal-Ex II, Fisher Scientific). The samples were rinsed in PBS and stored in 10% neutral buffered formalin until imaging. They were imaged in a µCT system (Viva-CT, Scanco Medical) at a 21.5 µm voxel size. Two VOIs were defined to analyze the vessels inside the defect only and inside plus directly adjacent to the defect periphery. The images were globally thresholded based on X-ray attenuation to segment the contrast-filled vasculature from surrounding tissues.

2.9. Statistical analysis

Data were analyzed by analysis of variance (ANOVA) conducted in Minitab® 15 (Minitab Inc., State College, PA). Pairwise comparisons were made using the Tukey multiple comparison procedure. The normality of the residuals was evaluated by the Anderson–Darling normality test. To detect the presence of any pattern in the residual distribution, they were plotted against fitted values. To maintain the constancy of error variance and normality of error terms, data were transformed according to the Box–Cox procedure, wherever required [48,49]. To investigate the effect of time on sequential *in vivo* µCT data, paired *t*-tests were performed. A *p*-value < 0.05 was considered statistically significant. All data are shown as mean ± standard error of mean (SEM).

3. Results

3.1. Nanofiber mesh tube characterization and placement

The nanofibers obtained by electrospinning were observed to be smooth and bead-free (Fig. 1A). The fibers ranged in diameter from 51 nm to 974 nm with 82% of the fibers between 50 nm and 150 nm. The mean and the median fiber diameter were calculated to be 154 nm and 107 nm respectively. Despite the high porosity of these

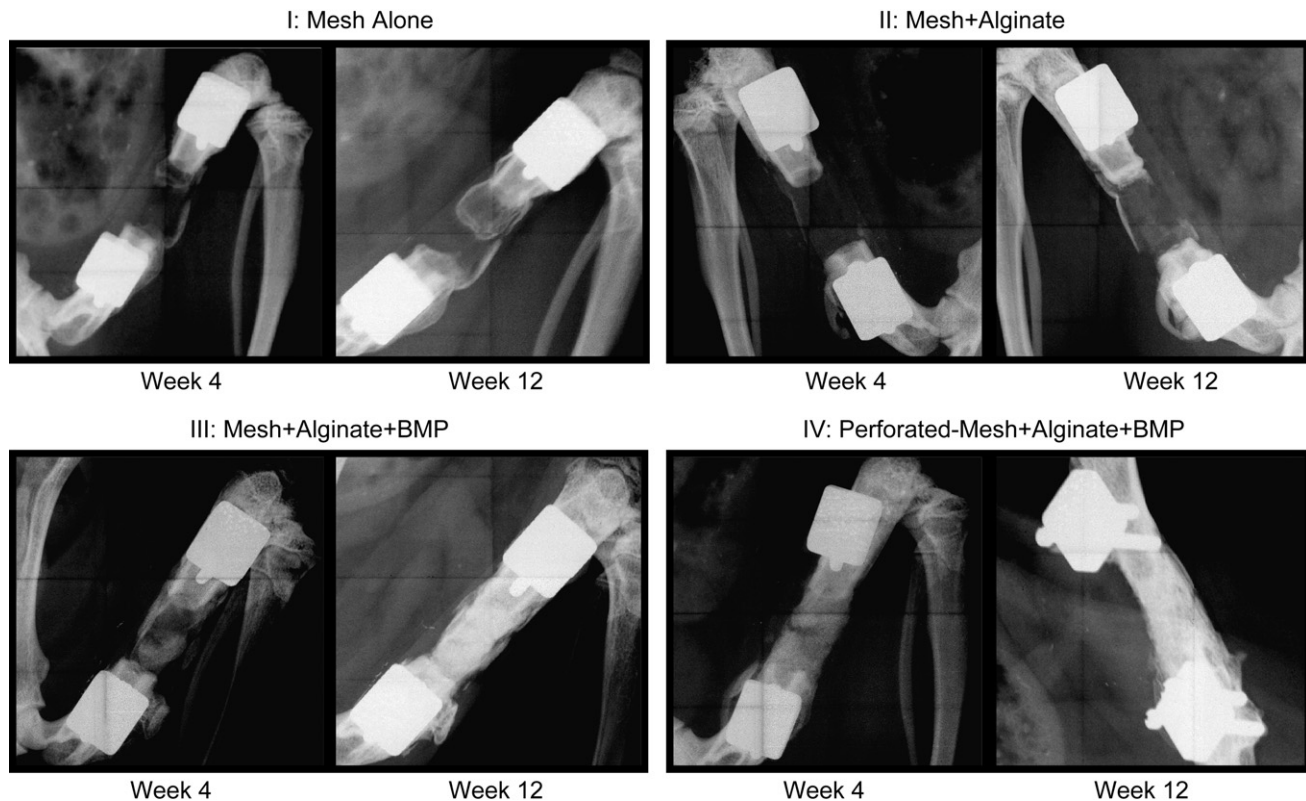


Fig. 2. Representative radiographs at 4 and 12 weeks. Defects in Groups I and II demonstrated small amount of bone formation, and did not bridge, even after 12 weeks. At week 4, defects in Groups III samples were infiltrated with considerable bony tissue, while Group IV samples exhibited the most robust mineralization. All samples in Groups III and IV were bridged with densely packed bone at week 12.

meshes (80–90%), the effective pore size was observed to be less than 5 μm . After 5 h of electrospinning, the mesh was found to be approximately 300–400 μm thick. This thickness was sufficient to provide a bending stiffness that prevented collapse of the mesh in solution. The thick nanofiber meshes were able to be wrapped tightly around a steel mandrel, and glued to form a tube (Fig. 1B and C). Due to the fast curing time of the UV glue, it was localized to the overlapping edges and did not seep to the rest of the mesh. The perforated meshes held the tubular structure well, and the holes accounted for 10% of the total surface area of the mesh tube. The nanofiber mesh tubes were deformed slightly to place them around the native bone ends of the segmental defect, but they regained their original shape due to the elasticity of the mesh. The overlapping ends and the surrounding musculature resulted in the tubes being stably located around the defect for the duration of the study (Fig. 1D and E). In some samples that were taken down after one week, the alginate was found to be still present inside the tube lumen, even in perforated tubes, with hematoma formation at the bone ends (Fig. 1F).

3.2. Alginate release kinetics

rhBMP-2 was encapsulated in alginate plugs, with each specimen containing 500 ng of the protein. After dissolving the alginate specimens on day 0, 275.5 \pm 15.6 ng rhBMP-2 was detected in the resulting solution. The release of bioactive rhBMP-2 from the alginate hydrogel specimens was monitored over a period of 21 days (Fig. 1G). The amount released in the buffer solution in active form by day 21 was 71.2 \pm 3.8 ng. The majority of the release took place within the first 7 days (98.6% of total released). We also assayed for the amount of rhBMP-2 retained in the gels by dissolving them at day 21, and found that 27.2 \pm 3.3 ng was still present in the gels.

3.3. Radiographs

Two-dimensional radiographs were taken at 4 and 12 weeks for qualitative assessment of bone healing (Fig. 2). Radiographs at the early time point of 4 weeks indicated that Groups I & II (Table 1) specimens had small amounts of bone formation, originating from the cut native ends and extending somewhat along the periphery. Group I samples were implanted with a nanofiber mesh tube alone, whereas Group II contained, in addition, alginate hydrogel inside the mesh tube. On the other hand, samples from Groups III and IV, in which 5 μg rhBMP-2 was delivered within alginate, demonstrated significant infiltration of mineralized tissue throughout the defect. Group IV specimens that were implanted with the perforated mesh tube exhibited the most robust mineralization. Group IV demonstrated the highest bridging rate (5/8) at the 4 week time point, whereas the remaining 3/8 defects were nearly bridged. Group III had none bridged, but 3/6 defects were nearly bridged. At 12 weeks, Groups I and II had still not achieved osseous union in any specimen, with most of the bony tissue formed on the periphery. In contrast, all specimens in Groups III and IV were completely bridged with densely packed bone.

3.4. *In vivo* μCT imaging

Animals were scanned in an *in vivo* μCT system at 4 and 12 weeks for quantifying bone formation (Fig. 3). The three-dimensional μCT images revealed that new bone formation in Groups III and IV occurred throughout the cross-section of the defect, whereas the small amount in Groups I and II appeared predominantly at the native bone margins and the defect periphery (Fig. 3A). The analysis of regenerated bone volumes indicated that Groups III and IV (Table 1) had significantly more (a ; $p < 0.05$) bone

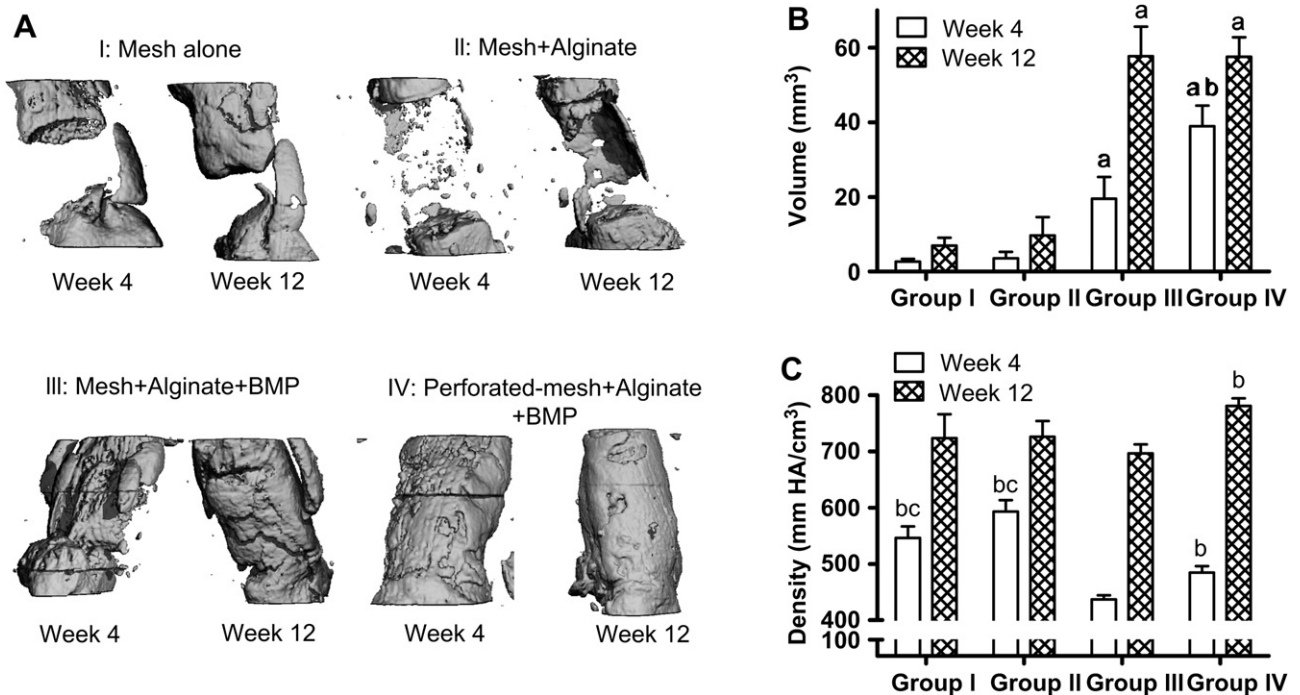


Fig. 3. μCT analysis of bone regeneration at 4 and 12 weeks. (A) μCT images illustrate that defects in Groups III and IV were filled with newly formed bone, while those in Groups I and II possessed limited new bone at the native bone ends and the defect periphery. (B) Quantification of regenerated bone volume revealed that the rhBMP-2 groups (Group III and IV) had significantly more bone formation than the groups without rhBMP-2 (Groups I and II), at both 4 and 12 weeks. Perforations in the nanofiber mesh tubes accelerated bone formation at 4 weeks (Group IV > Group III). (C) Local density of regenerated bone. At week 4, samples in Groups I and II demonstrated higher density than the other two groups. Density of Group IV samples was higher than those in Group III, at both time points (a – significantly different than Groups I and II, $p < 0.05$; b – significantly different than Group III, $p < 0.05$; c – significantly different than Group IV.).

formation in the defect compared to Groups I and II, at both time points (Fig. 3B). At 4 weeks, Group IV, implanted with the perforated mesh, had significantly more (b; $p < 0.05$) bone formation than Group III, which contained the mesh tubes without holes. However at 12 weeks, there was no difference in bone volumes between Groups III and IV. There was a significant increase in bone volumes with time in Groups I ($p = 0.048$), III ($p < 0.001$) and IV ($p = 0.001$), but not in Group II ($p = 0.08$). Group III ($37.65 \pm 2.22 \text{ mm}^3$) samples demonstrated the greatest increase in bone volume between 4 and 12 weeks, followed by Group IV ($20.02 \pm 2.96 \text{ mm}^3$). Compared to these two groups, Groups I ($3.96 \pm 1.40 \text{ mm}^3$) and II ($2.09 \pm 0.80 \text{ mm}^3$) had significantly less bone accumulation during the same period.

The local density of the newly formed bone within the defect was also calculated at 4 and 12 weeks (Fig. 3C). At 4 weeks, Groups I and II contained higher density bone than Groups III and IV (b and c respectively; $p < 0.05$). Group IV samples demonstrated a density higher than Group III, at both 4 and 12 weeks (b; $p < 0.05$). There was a significant increase in density with time for all groups from 4 to 12 weeks.

3.5. Biomechanical properties

Torsional testing was performed on extracted femora at 12 weeks to test their biomechanical properties (Fig. 4). Age-matched non-operated femora were also tested to obtain properties of native intact bone. The maximum torque and stiffness in torsion were calculated from the torque–rotation data. Groups III and IV had significantly higher (a; $p < 0.01$) maximum torque and stiffness compared to Groups I and II, as did the intact bone. There was no significant difference between Groups III and IV. However, compared to the intact bone, only Group IV samples had statistically equivalent maximum torque and stiffness, whereas Group III samples had significantly lower properties (b; $p < 0.05$). The mechanical properties for Group IV were on average approximately 75% of those for intact bone. Most of the samples in Groups III and IV failed at the center of the regenerated bone; a few failed at the interface of the native bone at the distal end. The non-bridged samples in Groups I and II did not fail at a particular location as the soft tissue simply twisted during the torsional test.

3.6. Histological analysis

Ground MMA sections were stained and analyzed for examining the regenerated tissue (Fig. 5A and B). The nanofiber mesh tube was partially degraded due to the MMA processing steps, but could still be detected around the defect. In Groups I and II, very little mineralized tissue was observed in the defect site at 12 weeks, similar to the radiographic and μCT results (Fig. 5A: I and II). The defects in these specimens were sparsely populated with fibrous tissue. The new bone formation was limited to the proximity of native bone ends and along the mesh tube. The end of the defects remained disconnected, with the capping of the native ends with bony tissue. The sections from Groups III and IV revealed extensive mineral deposition and bony bridging of the defects in these groups (Fig. 5A: III and IV). The newly formed bone was observed to be a combination of immature woven bone and mature lamellar bone. There was good continuity of the newly mineralized matrix with the native bone ends. Group IV, in particular, demonstrated the presence of a higher amount of lamellar bone, better integration at the native bone interface and reconstitution of marrow spaces. Residual alginate was evident within the defect, appearing as dark areas in histologic images. The higher magnification images of Groups III and IV indicated the presence of osteocytes embedded in lacunae and osteoblasts lining the new bone surfaces (Fig. 5B).

Histological analysis performed at 4 weeks revealed no evidence of cartilage tissue formation or endochondral ossification, indicating direct, intramembranous bone formation within the alginate gel (data not shown). The density maps obtained from the μCT indicate good correlation with histology sections (Fig. 5C). In addition, Group IV appeared to contain higher density mineralized tissue, which was distributed in a tubular pattern, similar to that of native cortical structure.

3.7. μCT -based angiography

Additional animals, implanted with rhBMP-2 identical to Groups III and IV in the long-term study, were euthanized at 3 weeks post-implantation, and their hind limb vasculature perfused with a radiopaque contrast agent. The femur and the surrounding soft tissues were imaged using μCT to quantify vascular ingrowth at an early time point preceding bone regeneration. Contours were drawn to define two VOIs. The first VOI included only the volume

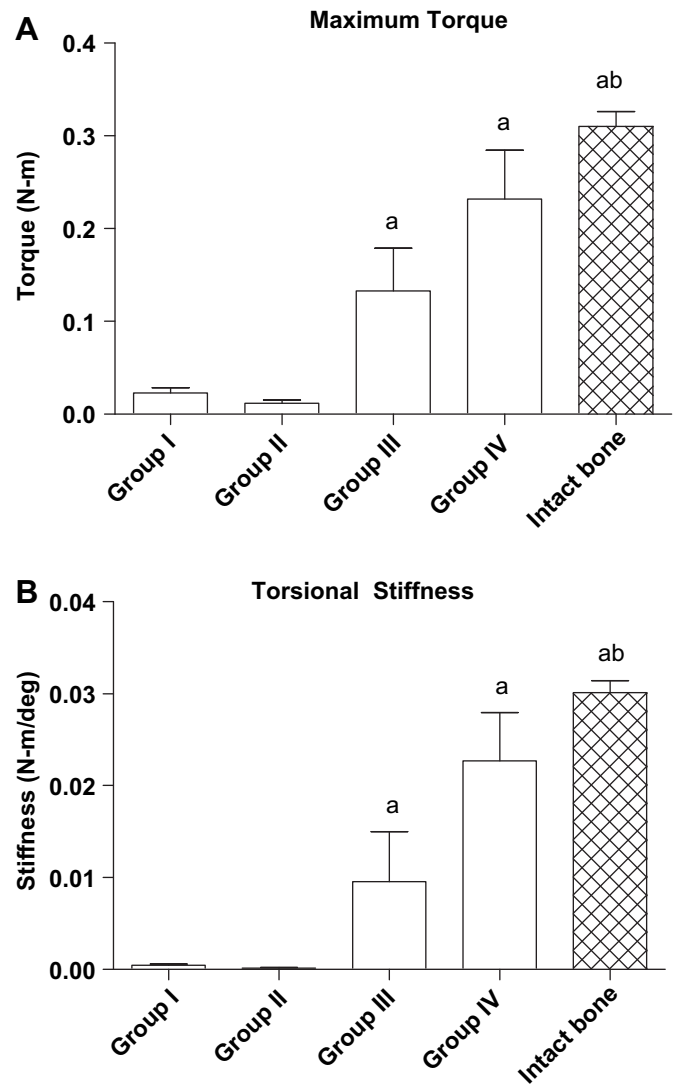


Fig. 4. Mechanical properties of femora at 12 weeks. (A) Maximum torque and (B) torsional stiffness. Mechanical properties in Groups III and IV were significantly higher than in Groups I and II. Compared to intact bones, Group III samples had significantly lower properties, whereas Group IV samples were statistically equivalent (a – significantly different than Groups I and II, $p < 0.01$; b – significantly different than Group III, $p < 0.05$). (I) Mesh alone, (II) Mesh with alginate, (III) Mesh with alginate containing rhBMP-2, (IV) Perforated mesh with alginate containing rhBMP-2.

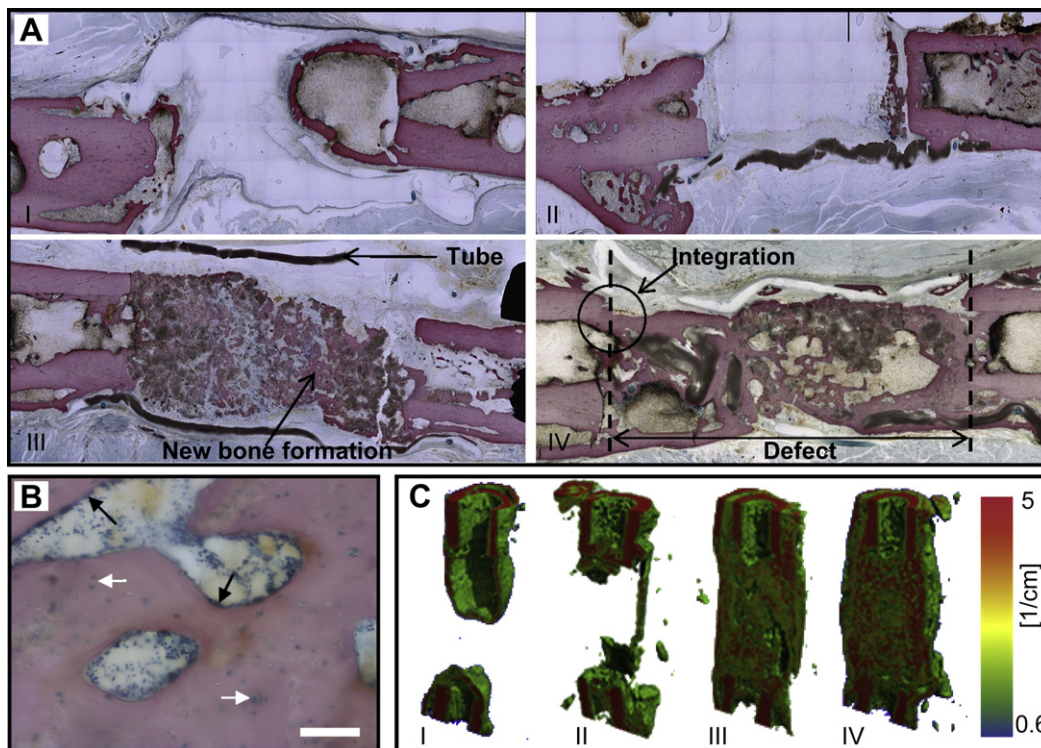


Fig. 5. (A) Ground sections were stained with Sanderson's rapid bone stain at 12 weeks (4× magnification). Defects in Groups I and II were sparsely populated with fibrous tissue, with the native ends capped with bony tissue. Defects in Groups III and IV had extensive bone deposition throughout the defect, with Group IV samples demonstrating better integration with the native bone. (B) Higher magnification section, representative of the newly formed bone in Groups III and IV (10× magnification). White arrows point to osteocytes embedded in lacunae. Black arrows point to osteoblasts lining the bone surface. Scale bar is 100 μm. (C) Density maps obtained from the μCT analysis at 12 weeks indicate good correlation with histology sections. The color scale to the right correlates to the attenuation of bone. Red color indicates higher density bone (higher attenuation), whereas green color represents lower density bone (lower attenuation). Compared to Group III, Group IV samples contained higher density bone, distributed along the native cortices. (I) Mesh alone, (II) Mesh with alginate, (III) Mesh with alginate containing rhBMP-2, (IV) Perforated mesh with alginate containing rhBMP-2.

inside the defect region, whereas the second contained both the defect and the periphery of the defect, termed the total VOI (Fig. 6). The analysis of the vasculature revealed the presence of vessels, both inside and outside the defect. The majority of the vascularity was observed in the periphery, as indicated by the significantly larger vessel volume in the total VOI ($a; p < 0.001$). There were no significant differences in vascular volume between Groups III and IV, in either the defect or the total VOI.

4. Discussion

The treatment of large osseous defects remains a challenge for orthopaedic surgeons. To address this problem, we have developed a growth factor delivery technique for the functional repair of large bone defects using an electrospun nanofiber mesh tube and alginate hydrogel. Tubular scaffolds constructed from nanofiber meshes were placed around segmental defects. Alginate hydrogel containing 5 μg rhBMP-2 was injected into the tubes and constrained within the defect site by the mesh tube. Our results demonstrate that this technique results in substantial bone formation and complete defect bridging. Importantly, samples implanted with both perforated mesh tube and rhBMP-2 containing alginate had statistically equivalent biomechanical properties to those of intact age-matched femora, indicating functional restoration of the limb function.

The majority of scaffolds proposed for bone reconstruction are structural scaffolds designed to support *in vivo* loads and provide a three-dimensional framework for cell attachment. They are examples of "hard scaffolds", usually made from slowly hydrolyzing

polymers or ceramics with unpredictable degradation [9,32,50]. Though they provide a structure for tissue growth, it is difficult to fine-tune their degradation rate to match the rate of tissue formation. Oest et al. reported that the use of such a scaffold hindered biomechanical restoration by occupying space and confining the bone formation to the pores and the periphery of the scaffold [11]. The use of structural scaffolds also precludes the use of an intramedullary pin for limb fixation, a technique frequently used by orthopaedic surgeons. In addition, the regular geometric shape of these scaffolds made them unsuitable to be placed inside fractures, which usually have irregular edges. Thin scaffold membranes have also been used for bone repair in a procedure termed guided bone/tissue regeneration [19,22]. In this technique, the membranes are positioned on the periosteal surface to provide a structure for bone formation. It has been argued that while 3-D scaffolds support the ingrowth of cells and tissue, the 2-D membranes may also protect the defect from soft tissue ingrowth and guide cell migration from the periosteum [14,51]. Since the membranes are placed on the periphery of the defect, they retain space for bone deposition throughout the defect. However, when a large mass of bone is lost, repopulating the entire defect with cells would be a challenge due to the presence of a large void, and the membrane may collapse due to soft tissue pressure.

Hydrogels are a class of highly hydrated matrices that enable cellular and tissue infiltration with relative ease [52]. Alginate hydrogels are an example of such a "soft scaffold" that can be deployed using minimally invasive procedures, conform to the shape of the defect and be manipulated by cells during tissue regeneration [53]. In addition, they can be used for sustained

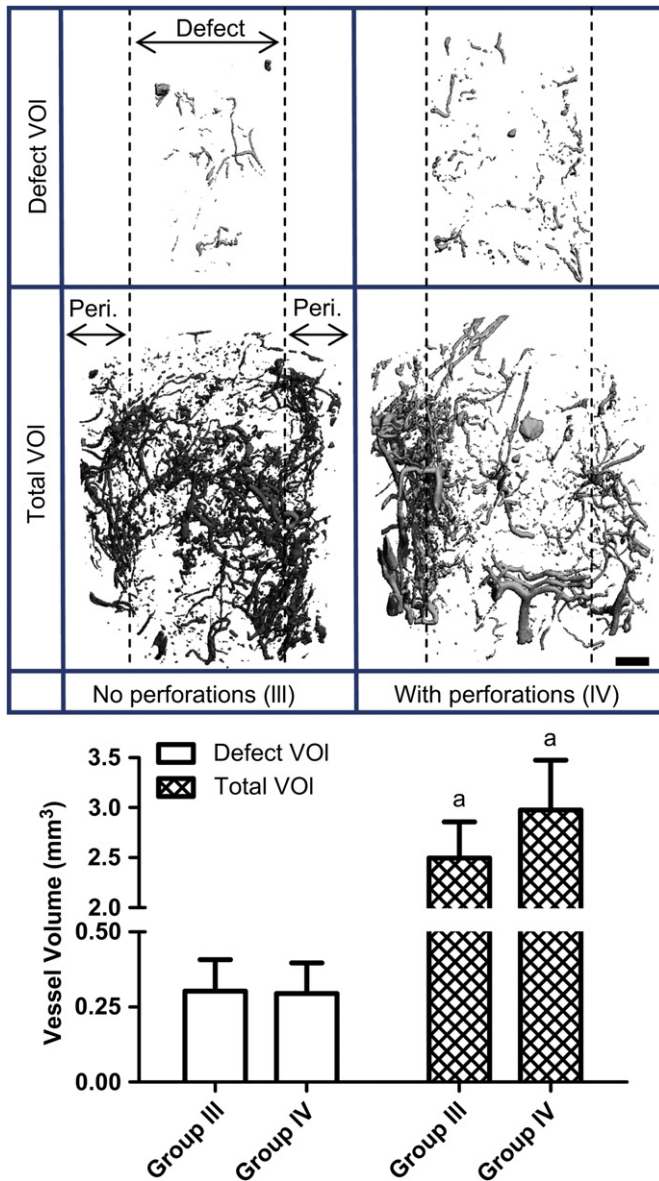


Fig. 6. Vascular ingrowth at the defect site at 3 weeks. Only Groups III and IV were included in this experiment. The defect VOI contains only the defect volume, whereas the total VOI contains the periphery of the defect in addition to the defect. The vascular volume was found to be significantly higher in the total VOI compared to the defect VOI. No significant differences were observed in the presence of perforations. Scale bar is 1 mm and applies to all images. Peri. – periphery of defect. (a – significantly different than the defect VOI; $p < 0.001$). (III) Mesh with alginate containing rhBMP-2, (IV) Perforated mesh with alginate containing rhBMP-2.

delivery of osteoinductive growth factors, a typical requirement for healing large defects. The primary concern with hydrogels is their inadequate mechanical stiffness, which causes them to deform easily under load.

In this study, we present a hybrid technique that utilizes both a nanofiber mesh membrane and an alginate hydrogel. The mesh tubes prevent soft tissue invagination into the defect and create a space for tissue regeneration. In addition, they potentially guide the migration of progenitor cells along the periosteal surface, and retain the osteogenic factors within the defect site. However, in this study, we observed that nanofiber mesh tubes, alone or in presence of alginate hydrogel without rhBMP-2, were not sufficient to bridge 8 mm segmental defects in rat femora. Without the presence of the

osteoinductive protein, the center was only sparsely populated by cells and bony tissue capped the ends of the defect. This is not surprising, since previous studies have demonstrated the need for a biologic stimulus for effective bone regeneration in this challenging model [11,12]. A series of studies have been performed to investigate the ability of polymer membranes to heal segmental diaphyseal defects [14,21,51,54]. Pineda et al. implanted porous polylactide membranes thermoformed into tubes in 1-cm defects in the rabbit radius, and observed bridging with new endosteal bone generation from the native bone ends [51]. However, in more challenging defects in the sheep tibia, bone grafting or a vascularized periosteal flap was needed, in addition to a membrane, to heal the defect [15,55].

In contrast, we found significantly higher bone formation with the delivery of rhBMP-2 in alginate hydrogel. All defects in the rhBMP-2 groups (Groups III and IV) were bridged by 12 weeks with densely packed, cellular mineralized tissue. This observed effect in the alginate/rhBMP-2 groups is hypothesized to be due to release of the protein from alginate, which occurs due to a combination of diffusion and gel degradation, or due to retention of the protein within the defect site by its binding to alginate. After dissolving the alginate samples on day 0, we observed that only 55.1% of the total rhBMP-2 (275.5 ng/500 ng) was detected by the ELISA. It is possible that the binding of some of the rhBMP-2 molecules to the alginate fibers masks the antibody binding site. This subset of rhBMP-2 molecules would not be detected by the ELISA, and therefore the actual amount of rhBMP-2 present in the hydrogels may be higher. Most of the rhBMP-2 that was released from the alginate did so within the first few days, perhaps due to the short alginate chains that are generated due to the irradiation of alginate. It is interesting to note that only 25.8% of the day 0 breakdown amount (71 ng/275.5 ng) was released in solution by day 21. Furthermore, 9.9% of the day 0 rhBMP-2 (27.2 ng/275.5 ng) was still present in the alginate at day 21, though the amount of the protein released at this time point was negligible. This suggests that a portion of the rhBMP-2 does indeed bind to the alginate fibers. It has been previously reported that alginate can reversibly bind proteins like BMP-2 through heparin-binding domains [56]. This bound rhBMP-2 may be available to invading cells at later time points. The binding of the protein to alginate could be an advantage, as this is thought to enhance the biological activity of the protein, perhaps by protection from premature degradation [57], and maintain a spatial cue during the tissue regeneration process. Future studies will further investigate the binding of rhBMP-2 to alginate by using radiolabeled rhBMP-2. Our calculations account for 98.2 ng (71 ng + 27.2 ng) out of 275.5 ng rhBMP-2 that was detected on day 0; the remaining rhBMP-2 may have been undetected by the ELISA and/or degraded over the 21 day incubation period. The RGD functionalized and short chain alginate used in this study also supported the robust penetration of osteogenic cells and tissue resulting in functional restoration.

The presence of perforations in nanofiber mesh tubes accelerated early bone formation and defect bridging. The utilization of *in vivo* μ CT scanning techniques permitted the sequential scanning of animals at multiple time points, and revealed that perforations in mesh tubes enhanced bone formation at 4 weeks. However, by 12 weeks, the group without perforations (Group III) had comparable bone volume to the group with perforations (Group IV). The differences in the bone deposition rate between 4 and 12 weeks could be attributed to the fact that at week 4, Group IV defects were almost filled with newly formed bone, whereas Group III defects still exhibited substantial space for bone formation. Compared to Group III, the density of the newly formed bone was significantly higher in Group IV. Also, only Group IV femora demonstrated functional restoration of biomechanical properties. These results indicate that perforations in the nanofiber mesh tube expedited bone formation, resulting in advanced bone remodeling and improved mechanical

properties. Gogolewski and coworkers used a perforated membrane along with autologous bone graft for treating segmental defects in sheep tibiae, and concluded that the perforations improved bone regeneration by enhancing graft survival [15,55]. They hypothesized that the perforations allow sufficient vascularization to develop, while limiting soft tissue ingrowth.

The improved bone repair due to perforations in the nanofiber mesh suggests that the bone regeneration process is mediated by interactions with the surrounding muscle tissue. For example, the perforations may enhance invasion of vascularity, migration of osteoprogenitor cells or diffusion of pro-regeneration soluble factors from the surrounding soft tissues into the defect region. We initially hypothesized that perforations improve vascular invasion, and employed a μ CT-based technique to quantitatively assess the vascularity in the early stages of bone regeneration [58]. However, our results indicated that the perforations did not have a significant effect on vascularity at the defect site. It is possible that the scan resolution was too low to detect the microvasculature in the developing bone [59]. The lack of differences in vascular regrowth due to the perforations suggests that some other interaction with the adjacent tissues may mediate the acceleration of bone formation. However, further studies are needed to elucidate the mechanisms behind this observed effect.

The current clinical technique for rhBMP-2 delivery involves soaking a collagen sponge with rhBMP-2 solution, which primarily relies on the adsorption of the protein to collagen [33]. However, a high dose of rhBMP-2 is required in this technique to obtain defect healing, possibly due to the suboptimal delivery kinetics. Numerous sustained delivery systems are being currently developed from natural and synthetic materials for reducing the high rhBMP-2 dose required clinically [13,60–64]. For example, Johnson et al. obtained the sustained release of rhBMP-2 without a large burst release by utilizing lipid-based microtubes [61]. A gelatin hydrogel engineered for the sustained release of rhBMP-2 resulted in the repair of a large ulnar defect [65]. On the other hand, Rizzi and coworkers reported that the physical linkage of rhBMP-2 to a recombinant protein–poly(ethylene glycol) hydrogel prevented optimal bone healing of murine cranial defects [66]. This was attributed to the inability of the bound rhBMP-2 to be released to provide a chemotactic signal and the insufficient degradation of the hydrogel matrix. By providing a sustained and localized release of rhBMP-2 and permitting robust cell infiltration, the hybrid alginate/nanofiber mesh system creates an environment conducive for bone regeneration. The 5 μ g dose utilized in this study is in the lower range of what has been reported (2–20 μ g) in similar models [11,13,67,68]. For example, in a 8 mm rat segmental defect model, 20- μ g of rhBMP-2 delivered on inactive demineralized bone matrix was required for defect bridging [67]. Future studies will compare our hybrid alginate/nanofiber mesh delivery system with the collagen scaffold rhBMP-2 delivery technique to provide a benchmark to the clinical standard.

5. Conclusions

A hybrid growth factor delivery system utilizing an electrospun nanofiber mesh and alginate hydrogel was presented in this study. This system resulted in complete bony bridging of challenging segmental bone defects in a rat model. Perforations accelerated the deposition of mineralized tissue and resulted in functional repair, possibly due to interactions of the surrounding soft tissues with the regenerating bone. The mesh tube alone, or in combination with alginate hydrogel, did not generate a significant repair response. Sustained delivery of rhBMP-2 via alginate hydrogel was required for substantial regeneration to occur. These results indicate that this hybrid technique may be clinically

useful for bone regeneration in the case of fracture non-unions and large bone defects.

Acknowledgements

This study was supported with funding from NIH R37 DE013033, NIH R01 AR051336, the Armed Forces Institute for Regenerative Medicine (AFIRM), and the Center for Advanced Engineering and Soldier Survivability (CABSS). The authors would like to thank Dr. Megan Oest for assistance with the segmental defect model and Dr. Craig L. Duvall for advice on μ CT-based angiography. We thank Angela Lin and Dr. Laura O'Farrell for assistance with μ CT analysis and animal welfare, respectively. We gratefully acknowledge Mehmet Bajin, Eric Deutsch, Dr. Tamim Diab, Chris Dosier, Mela Johnson, Jessica O'Neal, Hazel Stevens, Brent Uhrig, Jason Wang and Dr. Liqin Xie for their assistance in surgeries.

Appendix

Figures with essential color discrimination. Figs. 1, 5 and 6 in this article are difficult to interpret in black and white. The full color images can be found in the on-line version, at [doi:10.1016/j.biomaterials.2010.08.074](https://doi.org/10.1016/j.biomaterials.2010.08.074).

References

- [1] Borrelli Jr J, Prickett WD, Ricci WM. Treatment of nonunions and osseous defects with bone graft and calcium sulfate. *Clin Orthop Relat Res* 2003; 411:245–54.
- [2] Cypher TJ, Grossman JP. Biological principles of bone graft healing. *J Foot Ankle Surg* 1996;35(5):413–7.
- [3] Arrington ED, Smith WJ, Chambers HG, Bucknell AL, Davino NA. Complications of iliac crest bone graft harvesting. *Clin Orthop Relat Res* 1996;329:300–9.
- [4] Berrey Jr BH, Lord CF, Gebhardt MC, Mankin HJ. Fractures of allografts. Frequency, treatment, and end-results. *J Bone Jt Surg Am* 1990;72(6):825–33.
- [5] Wheeler DL, Enneking WF. Allograft bone decreases in strength in vivo over time. *Clin Orthop Relat Res* 2005;435:36–42.
- [6] Guldberg RE. Spatiotemporal delivery strategies for promoting musculoskeletal tissue regeneration. *J Bone Miner Res* 2009;24(9):1507–11.
- [7] Nerem RM. Tissue engineering: the hope, the hype, and the future. *Tissue Eng* 2006;12(5):1143–50.
- [8] Rose FR, Oreffo RO. Bone tissue engineering: hope vs hype. *Biochem Biophys Res Commun* 2002;292(1):1–7.
- [9] Salgado AJ, Coutinho OP, Reis RL. Bone tissue engineering: state of the art and future trends. *Macromol Biosci* 2004;4(8):743–65.
- [10] Guldberg RE, Oest ME, Dupont K, Peister A, Deutsch E, Kolambkar Y, et al. Biologic augmentation of polymer scaffolds for bone repair. *J Musculoskelet Neuronal Interact* 2007;7(4):333–4.
- [11] Oest ME, Dupont KM, Kong HJ, Mooney DJ, Guldberg RE. Quantitative assessment of scaffold and growth factor-mediated repair of critically sized bone defects. *J Orthop Res* 2007;25(7):941–50.
- [12] Rai B, Oest ME, Dupont KM, Ho KH, Teoh SH, Guldberg RE. Combination of platelet-rich plasma with polycaprolactone–tricalcium phosphate scaffolds for segmental bone defect repair. *J Biomed Mater Res A* 2007;81(4):888–99.
- [13] Chu TM, Warden SJ, Turner CH, Stewart RL. Segmental bone regeneration using a load-bearing biodegradable carrier of bone morphogenetic protein-2. *Biomaterials* 2007;28(3):459–67.
- [14] Meinig RP. Polylactide membranes in the treatment of segmental diaphyseal defects: animal model experiments in the rabbit radius, sheep tibia, Yucatan minipig radius, and goat tibia. *Injury* 2002;33(Suppl. 2):B58–65.
- [15] Gugala Z, Gogolewski S. Healing of critical-size segmental bone defects in the sheep tibiae using bioresorbable polylactide membranes. *Injury* 2002;33(Suppl. 2):B71–6.
- [16] Giardino R, Nicoli Aldini N, Fini M, Tanzi MC, Fare S, Draghi L, et al. Bioabsorbable scaffold for in situ bone regeneration. *Biomed Pharmacother* 2006;60(8):386–92.
- [17] Jung UW, Song KY, Kim CS, Lee YK, Cho KS, Kim CK, et al. Effects of a chitosan membrane coated with poly(lactic acid) and polyglycolic acid on bone regeneration in a rat calvarial defect. *Biomed Mater* 2007;2(3):S101–5.
- [18] Mengel R, Schreiber D, Flores-de-Jacoby L. Bioabsorbable membrane and bioactive glass in the treatment of intrabony defects in patients with generalized aggressive periodontitis: results of a 5-year clinical and radiological study. *J Periodontol* 2006;77(10):1781–7.
- [19] Eickholz P, Pretzl B, Holle R, Kim TS. Long-term results of guided tissue regeneration therapy with non-resorbable and bioabsorbable barriers. III. Class II furcations after 10 years. *J Periodontol* 2006;77(1):88–94.

- [20] Hutmacher D, Hutzler MB, Schliephake H. A review of material properties of biodegradable and bioresorbable polymers and devices for GTR and GBR applications. *Int J Oral Maxillofac Implants* 1996;11(5):667–78.
- [21] Meinig RP, Rahn B, Perren SM, Gogolewski S. Bone regeneration with resorbable polymeric membranes: treatment of diaphyseal bone defects in the rabbit radius with poly(L-lactide) membrane. A pilot study. *J Orthop Trauma* 1996;10(3):178–90.
- [22] Nasser NJ, Friedman A, Friedman M, Moor E, Mosheiff R. Guided bone regeneration in the treatment of segmental diaphyseal defects: a comparison between resorbable and non-resorbable membranes. *Injury* 2005;36(12):1460–6.
- [23] Mosheiff R, Friedman A, Friedman M, Liebergall M. Quantification of guided regeneration of weight-bearing bones. *Orthopedics* 2003;26(8):789–94.
- [24] Pham QP, Sharma U, Mikos AG. Electrospinning of polymeric nanofibers for tissue engineering applications: a review. *Tissue Eng* 2006;12(5):1197–211.
- [25] Murugan R, Ramakrishna S. Nano-featured scaffolds for tissue engineering: a review of spinning methodologies. *Tissue Eng* 2006;12(3):435–47.
- [26] Kolambkar YM, Peister A, Ekaputra AK, Hutmacher DW, Guldberg RE. Colonization and osteogenic differentiation of different stem cell sources on electrospun nanofiber meshes. *Tissue Eng Part A*; 2010.
- [27] Kim HW, Lee HH, Knowles JC. Electrospinning biomedical nanocomposite fibers of hydroxyapatite/poly(lactic acid) for bone regeneration. *J Biomed Mater Res A* 2006;79(3):643–9.
- [28] Yoshimoto H, Shin YM, Terai H, Vacanti JP. A biodegradable nanofiber scaffold by electrospinning and its potential for bone tissue engineering. *Biomaterials* 2003;24(12):2077–82.
- [29] Badami AS, Kreke MR, Thompson MS, Riffle JS, Goldstein AS. Effect of fiber diameter on spreading, proliferation, and differentiation of osteoblastic cells on electrospun poly(lactic acid) substrates. *Biomaterials* 2006;27(4):596–606.
- [30] Piskin E, Isoglu IA, Bolgen N, Vargel I, Griffiths S, Cavusoglu T, et al. In vivo performance of simvastatin-loaded electrospun spiral-wound polycaprolactone scaffolds in reconstruction of cranial bone defects in the rat model. *J Biomed Mater Res A* 2009;90(4):1137–51.
- [31] Kim KH, Jeong L, Park HN, Shin SY, Park WH, Lee SC, et al. Biological efficacy of silk fibroin nanofiber membranes for guided bone regeneration. *J Biotechnol* 2005;120(3):327–39.
- [32] Bruder SP, Kraus KH, Goldberg VM, Kadiyala S. The effect of implants loaded with autologous mesenchymal stem cells on the healing of canine segmental bone defects. *J Bone Jt Surg Am* 1998;80(7):985–96.
- [33] Swiontkowski MF, Aro HT, Donell S, Esterhai JL, Goulet J, Jones A, et al. Recombinant human bone morphogenetic protein-2 in open tibial fractures. A subgroup analysis of data combined from two prospective randomized studies. *J Bone Jt Surg Am* 2006;88(6):1258–65.
- [34] De Biase J, Capanna R. Clinical applications of BMPs. *Injury* 2005;36(Suppl. 3):43–6.
- [35] Chen RR, Mooney DJ. Polymeric growth factor delivery strategies for tissue engineering. *Pharm Res* 2003;20(8):1103–12.
- [36] Rose FR, Hou Q, Oreffo RO. Delivery systems for bone growth factors – the new players in skeletal regeneration. *J Pharm Pharmacol* 2004;56(4):415–27.
- [37] Garrison KR, Donell S, Ryder J, Shemilt I, Mugford M, Harvey I, et al. Clinical effectiveness and cost-effectiveness of bone morphogenetic proteins in the non-healing of fractures and spinal fusion: a systematic review. *Health Technol Assess* 2007;11(30):1–150.
- [38] Benglis D, Wang MY, Levi AD. A comprehensive review of the safety profile of bone morphogenetic protein in spine surgery. *Neurosurgery* 2008;62(5 Suppl. 2):ONS423–31.
- [39] Simmons CA, Alsberg E, Hsiong S, Kim WJ, Mooney DJ. Dual growth factor delivery and controlled scaffold degradation enhance in vivo bone formation by transplanted bone marrow stromal cells. *Bone* 2004;35(2):562–9.
- [40] Wee S, Gombotz WR. Protein release from alginate matrices. *Adv Drug Deliv Rev* 1998;31(3):267–85.
- [41] Augst AD, Kong HJ, Mooney DJ. Alginate hydrogels as biomaterials. *Macromol Biosci* 2006;6(8):623–33.
- [42] Lee KY, Peters MC, Anderson KW, Mooney DJ. Controlled growth factor release from synthetic extracellular matrices. *Nature* 2000;408(6815):998–1000.
- [43] Alsberg E, Anderson KW, Albeiruti A, Franceschi RT, Mooney DJ. Cell-interactive alginate hydrogels for bone tissue engineering. *J Dent Res* 2001;80(11):2025–9.
- [44] Alsberg E, Kong HJ, Hirano Y, Smith MK, Albeiruti A, Mooney DJ. Regulating bone formation via controlled scaffold degradation. *J Dent Res* 2003;82(11):903–8.
- [45] Rowley JA, Madlambayan G, Mooney DJ. Alginate hydrogels as synthetic extracellular matrix materials. *Biomaterials* 1999;20(1):45–53.
- [46] Sanderson C, Bachus K. Staining technique to differentiate mineralized and demineralized bone in ground section. *J Histotechnol* 1997;20(2):119–22.
- [47] Duvall CL, Taylor WR, Weiss D, Guldberg RE. Quantitative microcomputed tomography analysis of collateral vessel development after ischemic injury. *Am J Physiol Heart Circ Physiol* 2004;287(1):H302–10.
- [48] Box GEP, Cox DR. An analysis of transformations. *J R Stat Soc B* 1964;26:211–43.
- [49] Kutner MH, Nachtsheim CJ, Neter J, Li W. *Applied linear statistical models*. 5th ed. New York, NY: McGraw-Hill; 2005.
- [50] Hutmacher DW, Schantz T, Zein I, Ng KW, Teoh SH, Tan KC. Mechanical properties and cell cultural response of polycaprolactone scaffolds designed and fabricated via fused deposition modeling. *J Biomed Mater Res* 2001;55(2):203–16.
- [51] Pineda LM, Busing M, Meinig RP, Gogolewski S. Bone regeneration with resorbable polymeric membranes. III. Effect of poly(L-lactide) membrane pore size on the bone healing process in large defects. *J Biomed Mater Res* 1996;31(3):385–94.
- [52] Elisseff J, Puleo C, Yang F, Sharma B. Advances in skeletal tissue engineering with hydrogels. *Orthod Craniofac Res* 2005;8(3):150–61.
- [53] Drury JL, Mooney DJ. Hydrogels for tissue engineering: scaffold design variables and applications. *Biomaterials* 2003;24(24):4337–51.
- [54] Meinig RP, Buesing CM, Helm J, Gogolewski S. Regeneration of diaphyseal bone defects using resorbable poly(L/DL-lactide) and poly(DL-lactide) membranes in the Yucatan pig model. *J Orthop Trauma* 1997;11(8):551–8.
- [55] Gerber A, Gogolewski S. Reconstruction of large segmental defects in the sheep tibia using polylactide membranes. A clinical and radiographic report. *Injury* 2002;33(Suppl. 2):B43–57.
- [56] Peters MC, Isenberg BC, Rowley JA, Mooney DJ. Release from alginate enhances the biological activity of vascular endothelial growth factor. *J Biomater Sci Polym Ed* 1998;9(12):1267–78.
- [57] Silva EA, Mooney DJ. Spatiotemporal control of vascular endothelial growth factor delivery from injectable hydrogels enhances angiogenesis. *J Thromb Haemost* 2007;5(3):590–8.
- [58] Duvall CL, Taylor WR, Weiss D, Wojtowicz AM, Guldberg RE. Impaired angiogenesis, early callus formation, and late stage remodeling in fracture healing of osteopontin-deficient mice. *J Bone Miner Res* 2007;22(2):286–97.
- [59] Guldberg RE, Ballock RT, Boyan BD, Duvall CL, Lin AS, Nagaraja S, et al. Analyzing bone, blood vessels, and biomaterials with microcomputed tomography. *IEEE Eng Med Biol Mag* 2003;22(5):77–83.
- [60] Lutolf MP, Lauer-Fields JL, Schmoekel HG, Metters AT, Weber FE, Fields GB, et al. Synthetic matrix metalloproteinase-sensitive hydrogels for the conduction of tissue regeneration: engineering cell-invasion characteristics. *Proc Natl Acad Sci U S A* 2003;100(9):5413–8.
- [61] Johnson MR, Lee HJ, Bellamkonda RV, Guldberg RE. Sustained release of BMP-2 in a lipid-based microtube vehicle. *Acta Biomater* 2009;5(1):23–8.
- [62] Kokubo S, Fujimoto R, Yokota S, Fukushima S, Nozaki K, Takahashi K, et al. Bone regeneration by recombinant human bone morphogenetic protein-2 and a novel biodegradable carrier in a rabbit ulnar defect model. *Biomaterials* 2003;24(9):1643–51.
- [63] Prabakaran M, Mano JF. Chitosan-based particles as controlled drug delivery systems. *Drug Deliv* 2005;12(1):41–57.
- [64] Saito N, Okada T, Horiuchi H, Murakami N, Takahashi J, Nawata M, et al. Biodegradable poly-D,L-lactic acid-polyethylene glycol block copolymers as a BMP delivery system for inducing bone. *J Bone Jt Surg Am* 2001;83-A(Suppl. 1(Pt 2)):S92–8.
- [65] Yamamoto M, Takahashi Y, Tabata Y. Enhanced bone regeneration at a segmental bone defect by controlled release of bone morphogenetic protein-2 from a biodegradable hydrogel. *Tissue Eng* 2006;12(5):1305–11.
- [66] Rizzi SC, Ehrbar M, Halstenberg S, Raebler GP, Schmoekel HG, Hagenmuller H, et al. Recombinant protein-co-PEG networks as cell-adhesive and proteolytically degradable hydrogel matrices. Part II: biofunctional characteristics. *Biomacromolecules* 2006;7(11):3019–29.
- [67] Lieberman JR, Daluiski A, Stevenson S, Wu L, McAllister P, Lee YP, et al. The effect of regional gene therapy with bone morphogenetic protein-2-producing bone-marrow cells on the repair of segmental femoral defects in rats. *J Bone Jt Surg Am* 1999;81(7):905–17.
- [68] Yasko AW, Lane JM, Fellingner EJ, Rosen V, Wozney JM, Wang EA. The healing of segmental bone defects, induced by recombinant human bone morphogenetic protein (rhBMP-2). A radiographic, histological, and biomechanical study in rats. *J Bone Jt Surg Am* 1992;74(5):659–70.